Energy transfer, up-conversion and nonequivalent crystal field effects in the $KYP_4O_{12}:Pr^{3+}$ system

1989 J. Phys.: Condens. Matter 1 4673

(http://iopscience.iop.org/0953-8984/1/28/017)

J. Phys.: Condens. Matter 1 (1989) 4673–4686. Printed in the UK

Energy transfer, up-conversion and non-equivalent crystal field effects in the $KYP_4O_{12}:Pr^{3+}$ system

Michał Malinowski

Institute of Microelectronics and Optoelectronics PW, ul. Koszykowa 75, 00662 Warsaw, Poland

Received 4 October 1988, in final form 10 January 1989

Abstract. Under selective pulsed dye laser excitation in the $^1D_2$ state fluorescence of Pr^{3+} ions in KYP_4O_{12} has been studied. The presence of complex structures in the excitation and emission spectra associated with ion pairs and perturbed single ions is revealed. It is shown that in low concentration crystals most of the $^1D_2$ fluorescence originates from the perturbed Pr^{3+} ions. The kinetics of the $^1D_2$ decay is measured and discussed in terms of cross relaxation, energy transfer to traps and up-conversion processes. These results are in satisfactory agreement with the developed rate equation model. The contribution of short-range interaction, probably superexchange, in the quenching of $^1D_2$ fluorescence in strongly concentrated crystals is examined. The first observations of $^1D_2$ and up-converted $^3P_0$ emissions in stoichiometric Pr^{3+} phosphate are reported.

1. Introduction

Interest in dilute and stoichiometric rare earth (RE) phosphates has increased due to their potential application in mini-lasers (Huber 1980). Stoichiometric Nd^{3+} phosphates exhibit unusually weak concentration-dependent fluorescence quenching. This allows the active ion concentration to be very high without significant degradation of the lasing properties of the material. The concentration quenching characteristics of neodymium stoichiometric materials have been satisfactorily explained (Broer *et al* 1984, Lawson *et al* 1982, Malinowski 1986), but much less is known about the fluorescence of other RE ions in this type of material. Praseodymium stoichiometric crystals PrP_5O_{14} (Dornauf and Heber 1979, Szymański 1984), $LiPr_4O_{12}$ (Mazurak *et al* 1984), $KPrP_4O_{12}$ (hereafter abbreviated KPP; Malinowski *et al* 1986), $K_5PrLi_2F_{10}$ (Lempicki and McCollum 1979), as well as mixed Pr–Y systems, exhibit interesting luminescence properties.

Room-temperature luminescence of Pr^{3+} ions can originate from three metastable states: $^3P_1$, $^3P_0$ and $^1D_2$. Because of the different quenching mechanisms for these luminescences the relative intensities of the emission lines depend strongly on the active ion concentration (Szymański 1984, Malinowski *et al* 1986). In all investigated stoichiometric Pr^{3+} crystals there was a complete absence of emissions originating from the $^1D_2$ state. The concentration dependence of Pr^{3+} emission intensities and the quenching of $^1D_2$ fluorescence by cross relaxation in $Pr_xLa_{1-x}P_5O_{14}$ has been studied by Dornauf and Heber (1980). It has been shown that at 4.4 K spectral diffusion is absent

0953-8984/89/284673 + 14 $02.50

in this system and that the observed quenching can be attributed to the following cross relaxation channels between two Pr^{3+} ions.

$$[^1D_2(1), {}^3H_4(1)] \rightarrow [^1G_4(i), {}^3F_4(j)] \tag{1}$$

where the indices in parentheses denote the Stark levels of a given multiplet: index (1) is the lowest Stark component. The above equation describes processes that are quasi-resonant or assisted by the emission of low-energy ($<100\ cm^{-1}$) phonons. The dominant ion–ion interaction, determined in the framework of discrete host structure model, was found to be of the electric dipole–quadrupole type.

The goal of the present investigation was to determine whether other concentration-dependent processes other than quasi-resonant cross relaxation contribute to non-radiative de-excitation of the $^1D_2$ state. In this paper we present the results of an investigation of the fluorescence dynamics of the $KPr_xY_{1-x}P_4O_{12}$ system, and special attention is devoted to the stoichiometric compound $KPrP_4O_{12}$. For the first time $^1D_2$ emission in pure Pr^{3+} phosphate is observed and analysed. Some new results on the energy transfer leading to up-converted $^3P_0$ fluorescence are presented. This work also suggests a role for a short-range interaction in the energy transfer between nearby ions.

2. Experimental methods

Six samples of $KPr_xY_{1-x}P_4O_{12}$, of nominal concentrations $x = 1$, 0.85, 0.2, 0.03, 0.01 and 0.002 were studied in the course of the investigation. They were obtained in our laboratory (IMiO, Warsaw) using the method of Miyazawa *et al* (1979). The single crystals were of a good optical quality with typical dimensions of $3 \times 1 \times 1\ mm^3$. The crystals were checked by x-ray diffraction and x-ray fluorescence techniques. The crystal symmetry is monoclinic with a space group P2/1, the rare earth ions are located at sites of C_2 symmetry, and the impurity concentration, mostly Nd^{3+} and Gd^{3+} ions, was found to be lower than 40 ppm.

The single-crystal samples were mounted in a liquid He cryostat with a gas heating system to allow temperature variations from 4.4 to 77 K. Luminescence was excited at right angles to the detection system by a three-state Rhodamine 6G dye laser (10 ns pulse width, $0.1\ cm^{-1}$ band width) pumped by a second harmonic of a quantum model 481 Nd : YAG laser. To avoid any non-linear processes, during most of the experiment the dye laser output was kept below 30 μJ per pulse energy. The $^1D_2$ emission from the samples was collected, passed through a 1 m Hilger and Watts monochromator and then detected with a cooled GaAs photomultiplier tube. The signal was processed by an Ortec photon counting system. The experimental set-up was controlled by Tektronics 4051 graphic minicomputer and the decay curves were recorded by Intertechnique In 90 multichannel analyser.

3. Experimental results

3.1. Pr^{3+} spectra

Ground state $^3H_4(1)$ to $^1D_2(1)$ absorption measured in the $KPrP_4O_{12}$ crystal gave an oscillator strength of 1.5×10^{-8} (for the discussed transitions see also the energy level diagram of figure 9). This relatively high value, despite the strong forbiddenness of this

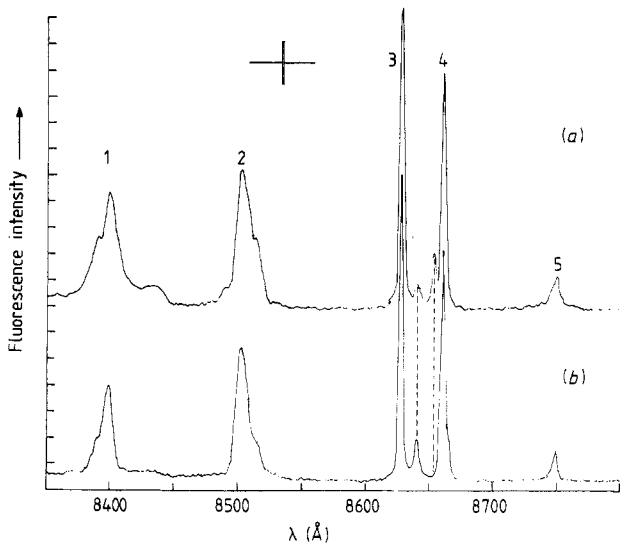

Figure 1. Time-integrated and time-resolved fluorescence spectra corresponding to the $^1D_2(1) \rightarrow {}^3F_2$ transition measured in $KPrP_4O_{12}$ at 4.4 K.

transition (Bartoli *et al* 1979), is probably due to the very low point symmetry of Pr^{3+} in tetrametaphosphates and allows efficient optical excitation with laser pulses of 30 μJ in energy, corresponding in the considered experimental conditions to about 3×10^6 J cm^{-3} excitation density. In all our experiments we pumped resonantly the lowest Stark component of the $^1D_2$ state and observed the non-resonant $^1D_2(1) \rightarrow {}^3F_2$ fluorescence. This configuration is favourable because of the large branching ratio for this transition (Malinowski *et al* 1986), the wide spectral separation from the exciting laser radiation, and the absence of any reabsorption.

Figure 1 shows the 4.4 K fluorescence spectra around the $^1D_2(1) \rightarrow {}^3F_2$ transition after broad-band resonant excitation into the $^1D_2(1)$ level of Pr^{3+} in $KPrP_4O_{12}$. Figure 1(*a*) shows the time-integrated spectrum; figure 1(*b*) shows the time-resolved (TR) fluorescence monitored with a time delay after the laser pulse of 1 μs and a gate width of 5 μs. Pr^{3+} is a non-Kramers ion and because of a very low C_2 site symmetry in the investigated system, the $(2J + 1)$-fold degeneracies of the free-ion terms are totally removed by the crystalline potential. Thus the $^3F_2$ level is split into five Stark components, which are clearly observed in the spectrum. However, some additional structure in the vicinity of the $^1D_2(1) \rightarrow {}^3F_2(3, 4)$ lines is also observed and in figure 1(*b*) the time characteristics of these peaks are different. Using the monochromator with maximally opened slits (corresponding to about 20 Å band width) the $^1D_2(1) \rightarrow {}^3F_2(3, 4)$ fluorescence was selected and monitored when the laser was tuned through the $^3H_4(1) \rightarrow {}^1D_2(1)$ absorption line. Figure 2 shows the peak positions and details of the excitation spectra at 4.4 K. From figure 2 it can also be seen that the $^3H_4(1) \rightarrow {}^1D_2(1)$ absorption line consists of two peaks separated by 11 cm^{-1} and a few less intense satellite lines. These two major lines presumably arise from the transitions of regular, intrinsic Pr^{3+} ions and from ions situated in strongly perturbed lattice sites, trap ions. The weak satellite line structure observed in the excitation spectra of diluted samples could be related to the existence of isolated ion pairs. It is interesting to note that the relative intensities of two major lines change with concentration; in stoichiometric $KPrP_4O_{12}$

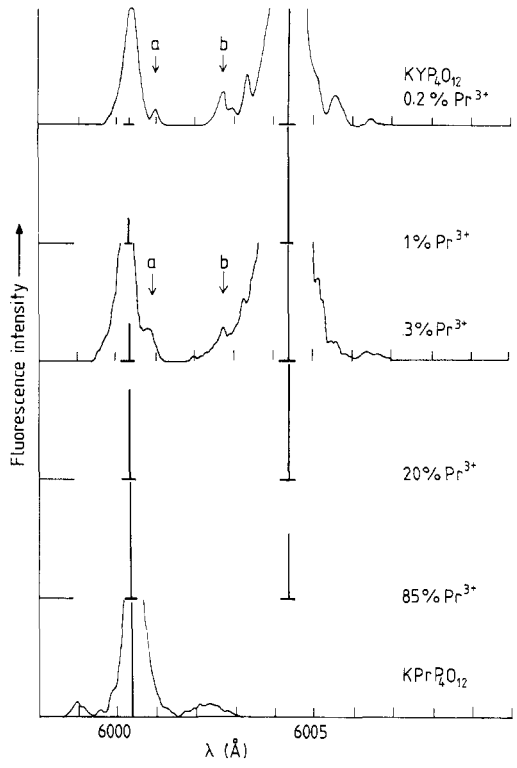

Figure 2. Excitation spectra of $^1D_2(1)$ fluorescence observed in six samples of $KYP_4O_{12}:Pr^{3+}$ of different nominal concentrations. The stick diagrams represent the relative integrated intensities of the regular and non-regular Pr^{3+} ion emission. Well resolved satellite lines are labelled by small letters. $T = 4.4$ K.

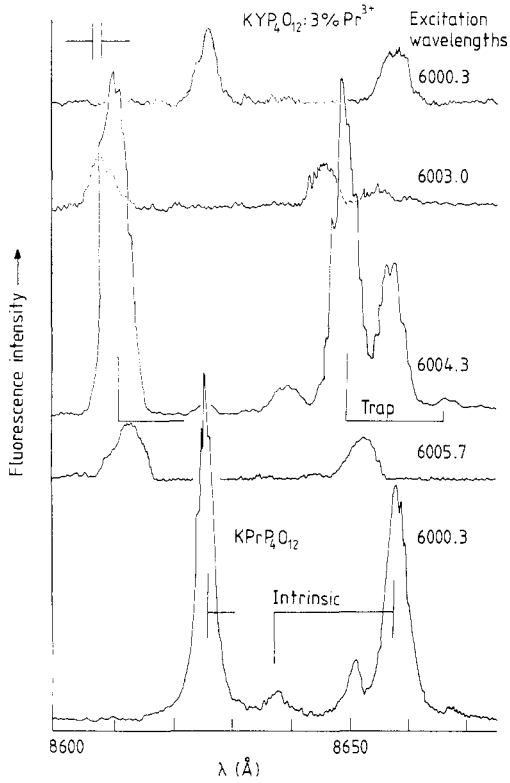

Figure 3. Fluorescence spectra of the $^1D_2(1) \rightarrow {}^3F_4(3,4)$ transition in $KYP_4O_{12}:3\%Pr^{3+}$ after selective excitation at various wavelengths (in Å). $T = 4.4$ K.

crystals the 6000.4 Å (16665.5 cm^{-1}) transition dominates, but its intensity falls in the low concentration samples where the line around 60043 Å (16654.7 cm^{-1}) dominates. This was confirmed by our low-temperature absorption measurements. The half-widths of the higher- and lower-energy peaks are 0.8 cm^{-1} in KPP and 1.3 cm^{-1} in $KYP:0.2\%Pr^{3+}$, respectively. For intermediate concentrations the low-energy lines are nearly twice as large as the high-energy ones. Most of the satellites appearing in the excitation spectra have laser-resolution-limited, concentration-independent widths of about 0.2 cm^{-1}.

In order to associate the observed fluorescence frequencies with corresponding excitation lines, the selectively excited fluorescence spectra were also recorded (figure 3). In pure KPP intrinsic ion fluorescence dominates ($\lambda_{exc} = 6000.4$ Å), although some weak features resulting from the perturbed ions excited by energy transfer are also observed. The back transfer manifests itself in the weak intrinsic emission from the directly excited trap ions ($\lambda_{exc} = 6004.3$ Å). With the dye laser tuned to the satellite absorption a new set of fluorescence lines are observed, slightly shifted in energies from the intrinsic ion value. Finally, we note that each emission line of the spectrum presented

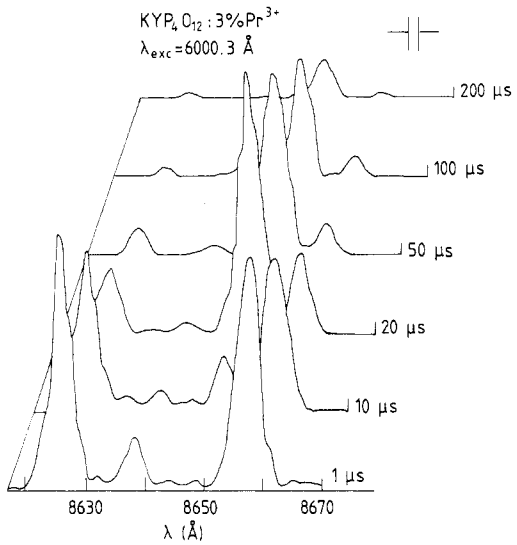

Figure 4. Time-resolved fluorescence spectra of the $^1D_2(1) \rightarrow {}^3F_4(4)$ transition in KYP_4O_{12}:3% Pr^{3+} after selective excitation of regular ions. T = 4.4 K.

in figure 3 provides a distinct excitation spectrum showing mainly the Stark splittings of the $^1D_2$ state of each perturbed Pr^{3+} ion.

3.2. The fluorescence dynamics

To examine any possible energy transfer between Pr^{3+} ions we used TR spectroscopy and measured $^1D_2(1) \rightarrow {}^3F_2(3, 4)$ spectra as a function of time in the range 1–200 μs after the excitation pulse. The excitation was in the intrinsic ions absorption. The time evolution of the $^1D_2$ emission illustrated in figure 4 is quite pronounced. With a 1 μs delay the intrinsic fluorescence dominates, and it almost vanishes at longer times when the growth of trap emission is observed. This process was also studied directly by monitoring the emission decay after selective excitation.

Three types of experiments were performed. First, with the dye laser tuned to the intrinsic ion absorption selected by the monochromator, the regular (8657 Å) and trap (8650 Å) fluorescences were recorded. Then, after direct excitation at 6004.3 Å the trap emission was recorded. Finally, the fluorescence resulting from the excitation of the two intense satellite lines was examined. Results of these experiments for KYP:3% Pr^{3+} are presented in figure 5. It can be noted that the decay of the intrinsic emission decreases as the sum of two exponential functions, one fast and one slow, with characteristic time constants of about 15 μs and 180 μs, respectively. The trap decay consists of a fast rise-time (approximately equal to the observed initial decay of the intrinsic ions) and then decreases nearly exponentially with a time constant of 200 μs. The initial rise-time becomes shorter with increasing temperature and at about 30 K disappears completely. When the satellite lines were pumped the emission decay was faster and strongly non-exponential.

The intrinsic ion emission as a function of temperature and Pr concentration has been also measured on an extended time scale and is presented in figure 6. The 4.4 K decay curves are characterised by an initially fast, non-exponential part that reflects the direct transfer to acceptors located at various distances from the donor ions. The initial part is followed by an exponential part with a decay rate approaching, for long times,

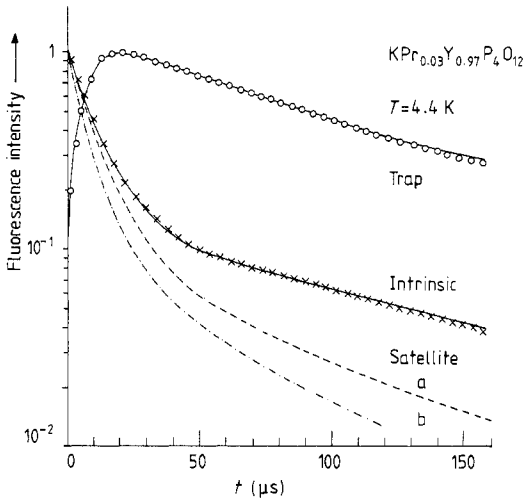

Figure 5. Time evolution of the regular (×) and non-regular (○) $^1D_2$ emissions in KYP_4O_{12}:3% Pr^{3+} after selective excitation of regular ions. The points represent experimental data; full curves are theoretical calculations using equations (4) and (5). See text for details.

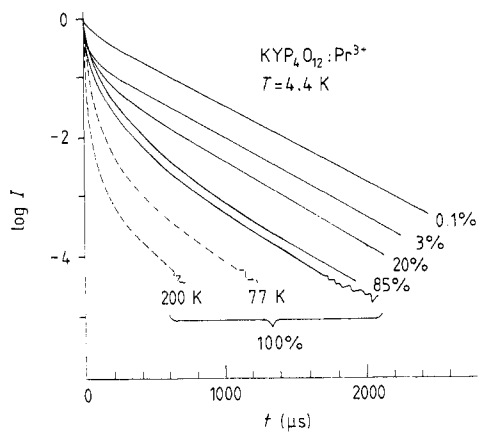

Figure 6. Fluorescence decay of regular ions observed from samples of $KYP_4O_{12}:Pr^{3+}$ at 4.4 K. Temporal variations of the $^1D_2$ emission in stoichiometric $KPrP_4O_{12}$ crystals measured at 77 and 200 K are represented by the broken curve.

the radiative rate, $\gamma_r = 2.9 \times 10^3\ s^{-1}$. At higher temperature the decay curves of the intrinsic system exhibit the same form, although the long-time exponential decay is much faster than the radiative one.

3.3. Anti-Stokes fluorescence

It was found that the blue lines resulting from the $^3P_0 \rightarrow {}^3H_4$ transitions were generated through the excitation of the $^1D_2(1)$ state. The time-integrated (TI) and TR excitation spectra of this anti-Stokes (or up-converted) emission were recorded when collecting the total $^3P_0$ (20769 cm^{-1}) fluorescence and tuning the laser frequency over the $^1D_2(1)$ absorption band (figure 7). For comparison, TI excitation spectra of the yellow $^1D_2$ fluorescence are also shown. In both investigated samples, i.e., $x = 0.3$ and 1, the TI spectra of $^3P_0$ and $^1D_2$ fluorescence have the same form. However, the spectra recorded with an integration gate of 2 μs positioned 2 μs after the excitation pulse exhibit different features. In the stoichiometric KPP the up-conversion signal appears after excitation of the main line when in the diluted KYP:3%Pr^{3+} system only satellites produce the $^3P_0$ fluorescence and the main line appears with increasing time delay.

The temporal evolution of the blue emission is presented in figure 8, the decay is generally non-exponential with a time constant at short time of about 10 μs and a very fast rise-time of <0.5 μs and about 4 μs in the case of KPP and KYP:3%Pr^{3+}, respectively. Excitation of the centre of absorption line in KPP results in the intense, delayed fluorescence with a rise-time constant of 25 μs and characteristic decay time of 110 μs. This type of fluorescence is not observed when exciting the satellites. By comparing the integrated excitation spectra of the $^3P_0$ and $^1D_2$ fluorescence, the overall efficiency of the up-conversion process has been estimated to be 2.6% and 0.5% for

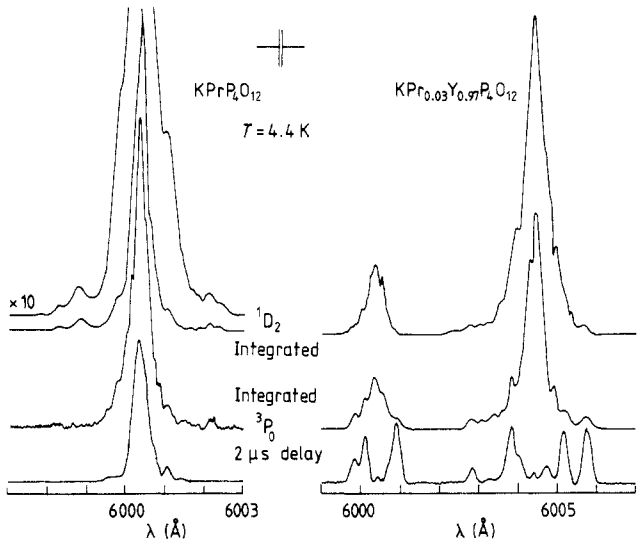

Figure 7. Time-resolved and time-integrated excitation spectra of up-converted $^3P_0$ fluorescence. For comparison, time-integrated excitation spectra of $^1D_2$ emissions in the investigated samples are also presented.

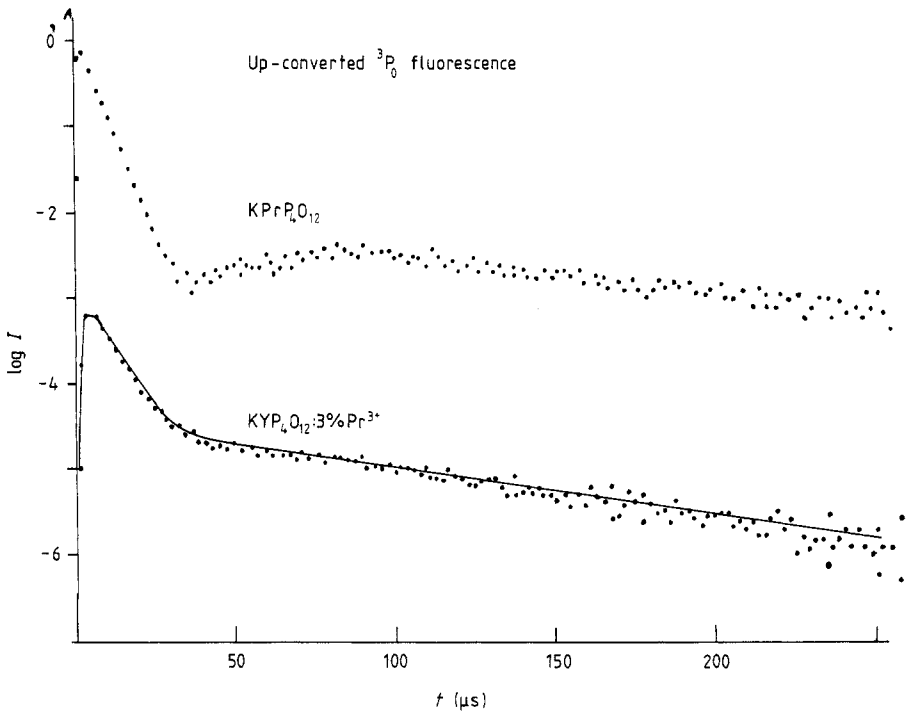

Figure 8. Time evolution of up-converted $^3P_0$ fluorescence observed in samples of KYP_4O_{12}: 3% Pr^{3+} and $KPrP_4O_{12}$ after excitation of regular ions. The points represent the experimental data; the full curve is the theoretical calculations using equation (14). (I is given in arbitrary units.)

KPP and KYP:3%Pr^{3+}, respectively. Finally, it was found that the blue fluorescence intensity has a quadratic dependence on the laser input power.

4. Discussion

4.1. Pr^{3+} spectra

The 4.4 K excitation spectra of the Pr^{3+} fluorescence in KPP presented in figure 2 show some weak features around the main $^3H_4(1) \rightarrow {}^1D_2(1)$ transition at 6000.3 Å. As in the case of stoichiometric Nd^{3+} and Sm^{3+} phosphates, this is interpreted in terms of some weakly perturbed ions whose energy is shifted from the intrinsic ion value. This perturbation is due to the presence of small quantities of rare earth impurities, probably Nd and Gd ions mentioned before. Since Pr^{3+} and Y^{3+} have different ionic radii, 1.09 Å and 0.93 Å, respectively, doping KPP with Y ions produces microscopic lattice distortions that result in an increase in the inhomogeneous line width, which shows its maximum for $x = 0.5$. It is also observed that with increased Y^{3+} doping levels a strong new line appears at 6004.3 Å. Its intensity increases with Y concentration, suggesting the creation of a concentration-dependent Pr^{3+} site in the mixed $KPr_xY_{1-x}P_4O_{12}$ system. Assuming the same oscillator strengths for regular and non-regular ion emissions, it appears that in the dilute crystals the observed fluorescence originates mostly from the non-regular Pr^{3+} ions.

The appearance of additional lines in the emission spectra of RE phosphates has been reported by Dornauf and Heber (1979) and Malinowski (1986), and the dependence of the line position on crystal composition was also observed by Malinowski *et al* (1988) in the Sm^{3+} system. The 9 cm^{-1} shift of the absorption line position in $KSmP_4O_{12}$ with respect to mixed $KSm_{0.01}Y_{0.99}P_4O_{12}$ was found. Similarly, a 12 cm^{-1} difference between the $^3P_0$ and $^1D_2(1)$ level positions in PrP_5O_{14} and $Pr_{0.01}La_{0.99}P_5O_{14}$, has been reported by Dornauf and Heber (1979). It seems that this particular situation in mixed crystalline phosphates is not only related to the difference in ionic radii between constituent and diluting ions. No changes in Pr^{3+} line position were found in the Pr(1.09 Å)–Er(0.96 Å) system (Malinowski 1989) although they were observed in Pr(1.09 Å)–Nd(1.08 Å) (Malinowski and Stręk 1987), Pr(1.09 Å)–Y(0.93 Å) and Sm(1.04 Å)–Y(0.93 Å) crystals (Malinowski *et al* 1988).

Weak satellite lines were observed in the spectra of all samples. As discussed earlier, in the strongly diluted systems the satellites result from isolated ion pairs in the nearest-neighbour positions. Analysing the well resolved satellite 'a' lying 2.5 cm^{-1} on the low-energy side of the intrinsic ion transition its quadratic intensity dependence on Pr^{3+} concentration was found. It thus seems reasonable to correlate this line with the Pr–Pr pair.

From the comparison of the integrated satellite 'a' intensity with that of the central line the twofold coordination of this pair was deduced suggesting its first- or second-neighbour origin. With excited level energy lying 11 cm^{-1} below the intrinsic (donor) ion value the irregular Pr^{3+} ions act as radiative traps (acceptors) for the $^1D_2(1)$ excitation. From the TRS results presented in figure 4 it is clear that the trap levels are populated by the energy transfer process originating from the excited intrinsic ions. The probability of upward transfer increases rapidly from 4.4 K to 25 K proportionally to $\exp(-\Delta E/kT)$ and above about 25 K the intrinsic and trap ions populations are thermalised. At 4.4 K, however, the intrinsic and trap emissions show a distinct excitation spectra, suggesting

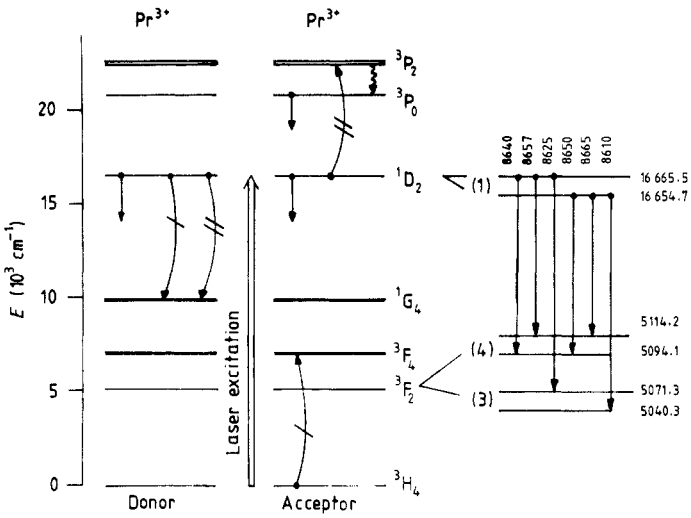

Figure 9. Schematic energy level diagram of Pr^{3+} ions in KYP_4O_{12} explaining the observed cooperative ion processes and the structure of the fluorescence and excitation spectra.

a strong localisation of the optical excitation and weak excitonic behaviour in this material.

A schematic energy level diagram explaining the observed processes in $KPr_xY_{1-x}P_4O_{12}$ system is presented in figure 9. On the right of the figure the details of the $^1D_2(1) \rightarrow {}^3F_2(3, 4)$ transition are interpreted.

4.2. Fluorescence dynamics

The rate equations describing the populations N of intrinsic 2 and trap 2′ levels after excitation into level 2 and assuming the same radiative transition rates for these levels are

$$dN_2/dt = -W_2N_2 - W_{t2}N_2 + W_bN_{2'} \tag{2}$$

$$dN_{2'}/dt = -W_2N_{2'} - W_bN_{2'} + W_{t2}N_2 \tag{3}$$

where W_{t2} and W_b are the time-independent transfer and back-transfer rates, respectively. With the initial conditions $N_2(0) = N_{20}$ and $N_{2'}(0) = 0$, the solutions are

$$N_2 = \frac{N_{20}}{W_{t2} + W_b + 2W_2} \times \{W_b \exp(-W_2t) + W_{t2} \exp[-(W_2 + W_{t2} + W_b)t]\} \tag{4}$$

$$N_{2'} = \frac{N_{20}W_{t2}}{W_{t2} + W_b + 2W_2} \{\exp(-W_2t) - \exp[-(W_2 + W_{t2} + W_b)t]\}. \tag{5}$$

From equations (4) and (5) it is clear that the intrinsic and trap ions decay as a sum and a difference of two exponential functions respectively. This is consistent with our observations of the decay curves in low concentration samples (see figures 5 and 6). In the concentrated crystals, however, due to the efficient direct transfer to a large number

of acceptors and due to cross relaxation the initial decay is no longer exponential. From equation (4) the initial fast intrinsic decay represents direct transfer to traps, its relative intensity changes as the ratio W_{t2}/W_b, which is strongly temperature dependent.

At long times after the excitation pulse the observed decay of the intrinsic Pr^{3+} emission recorded at 4.4 K approaches a single exponential. Since at 4.4 K the decay rate of the exponential tail is not much faster than the radiative rate ($2.9 \times 10^3\ s^{-1}$) of the intrinsic emission it could be supposed that at low temperatures a direct transfer to acceptor dominates the coupling mechanism. Above 30 K the donor decay is non-exponential for relatively short times after the excitation pulse and for long times the decay becomes exponential with a decay rate shorter than the radiative rate. We therefore conclude that we are dealing with a three-dimensional diffusion-limited migration in this temperature region. No emission from traps was observed above 30 K.

Using the values for W_{t2} and W_b as adjustable parameters the experimental decay curves were fitted to equations (4) and (5). This led in the low-concentration samples $x < 0.2$ to $W_{t2} = 7.7 \times 10^4\ s^{-1}$ and $W_b = 1.5 \times 10^4\ s^{-1}$. Figure 5 shows the theoretical fit for the KYP : 3% Pr^{3+} decay curves at 4.4 K. For $x = 0.2, 0.85$ and 1 samples the observed decay is strongly non-exponential for short times making the fit to equations (4) and (5) no longer possible. The fact that the fluorescence asymptotically approaches a single exponential decay with the isolated ion lifetime indicates that a short-range interaction is involved. In the absence of donor–donor transfer the temporal evolution of donor fluorescence in the presence of traps has been given by Huber (1979) in the form

$$f(t) = \exp(-\gamma_r t) \times \prod_i [1 - x + x \exp(-X_{0i} t)] \tag{6}$$

where X_{0i} is a transfer rate between a donor at site 0 and acceptor at site i, Π runs over all the lattice sites. X_{0i} in equation (6) is a function of donor–acceptor distance R_{0i} and in the approximation of electric multipolar interaction is given by

$$X_{0i} = X_{01}(R_{01}/R_{0i})^s \tag{7}$$

with X_{01} and R_{01} the nearest-neighbour transfer rate and distance, respectively, and $s = 6$, 8 and 10 for dipole–dipole, dipole–quadrupole and quadrupole–quadrupole interactions, respectively. For the case of energy transfer by exchange,

$$X_{0i} = X_{01} \exp[-\gamma(R_{01} - R_{0i})] \tag{8}$$

where γ is related to the effective Bohr radius l, $\gamma = 2/l$. In the limit of fast donor–donor transfer, equation (6) predicts a single exponential with a time constant given by Broer *et al* (1984) as

$$\tau_f = \left(\gamma_r - x \sum_i X_{0i}\right)^{-1} \tag{9}$$

where X_{0i} could be expressed by equations (7) or (8). The value of the nearest-neighbour transfer rate was derived from our room temperature data under the assumption of fast donor–donor transfer. From figure 10 the quasi-linear quenching rate dependence on Pr^{3+} concentration could be deduced (assuming dipole–quadrupole interaction suggested by Dornauf and Heber (1980)), resulting in a nearest-neighbour transfer rate of $X_{01} = 6.2 \times 10^4\ s^{-1}$ (for $x < 0.2$). It is also interesting to note that with increasing Pr^{3+} ion concentration, the decay time shortens and becomes temperature dependent, suggesting that concentration quenching is temperature dependent for $x > 0.2$. The value of X_{01} was also evaluated by our measurements on ion pairs. Assuming that the pair lifetime is

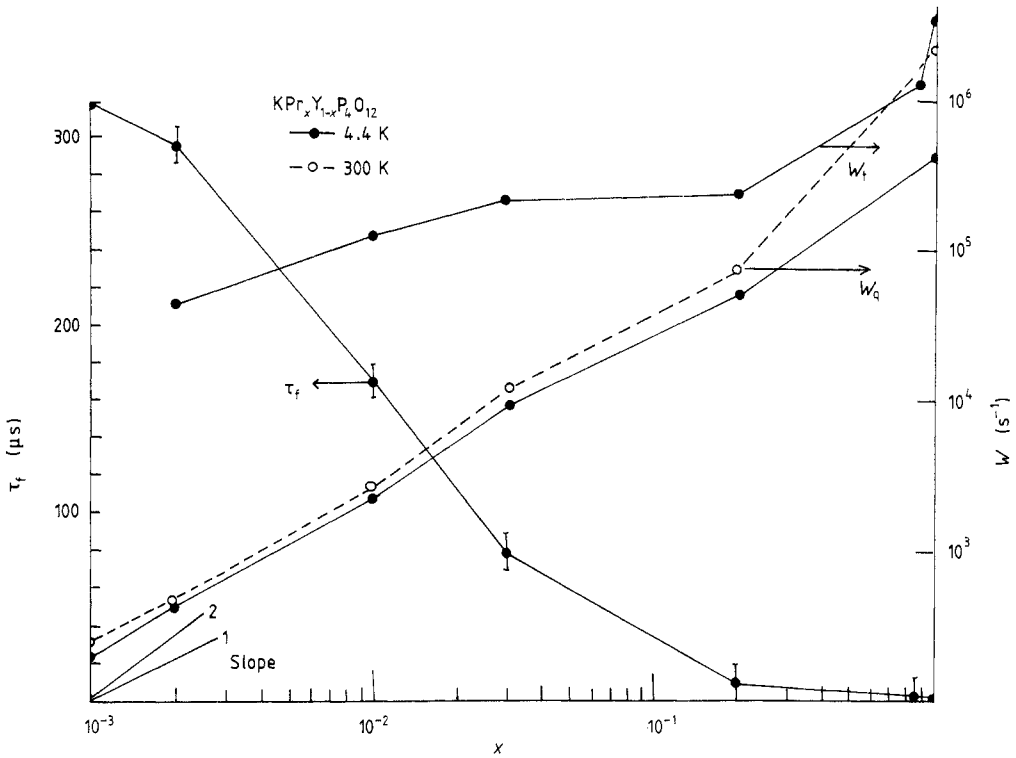

Figure 10. Variations in the $^1D_2$ fluorescence lifetime τ_f, quenching rate W_q and the up-conversion transfer rate W_t as a function of the active ion concentration x.

due to cross relaxation between an excited and unexcited Pr^{3+} ion the donor–acceptor transfer rate X_a of the pair 'a' (see figure 2) is given by

$$X_a = 1/\tau_a - \gamma_i \tag{10}$$

where γ_i is the decay rate of the intrinsic, isolated ion and τ_a is the pair lifetime. Taking the measured values of τ_a and γ_i, the quenching rate was found to be concentration independent up to $x = 0.2$ and has a value of $X_a = 7.1 \times 10^4\ s^{-1}$. This is in a reasonable agreement with the value deduced from room-temperature measurements. The agreement is even better if we take into account the differences in ion distances due to changes in lattice size when Y^{3+} is substituted by Pr^{3+}. This leads to a nearest-neighbour quenching rate in strongly diluted system of $X_{01} = 6.8 \times 10^4\ s^{-1}$. By using $\gamma_r = 2.9 \times 10^3\ s^{-1}$ and $X_{01} = 6.8 \times 10^4\ s^{-1}$ the experimental decay was fitted to equation (6) in the approximation of dipole–quadrupole interaction (Dornauf and Heber 1980). The first 188 neighbours of an excited ion residing in a sphere of 18 Å radius were included in the calculations. For concentrated samples, $x = 0.2, 0.85$ and 1, the calculated curves showed large deviations from experiment. The fit was better for dilute KYP : Pr^{3+}, although the initial fast decay over more than one decade was never predicted nor when using $s = 8$ neither for $s = 10$.

Finally, the model assuming short-range exchange interactions for the eight nearest neighbours (first four pairs) $R_{0i} = 6.62, 6.89, 6.99$ and 7.01 Å (see also Malinowski and Stręk 1987) and long-range dipole–quadrupole ($s = 8$) interactions for more distant ions

was used. In this case the agreement between theory and experiment was greatly improved, suggesting the simultaneous contribution of these two mechanisms to Pr^{3+} fluorescence quenching in the investigated system. From an inspection of the potassium metaphosphate structure, however, it seems very unlikely that exchange processes occur because of large interionic distances and the fact that this superexchange occurs via more than one O^{2-} ligand (Hong 1975).

4.3. Anti-Stokes fluorescence

Because of the quadratic dependence of the anti-Stokes $^3P_0$ fluorescence on excitation energy it could be concluded that we are dealing with a two-ion process. The $^3P_0$ luminescence arising after excitation of the $^1D_2$ state is interpreted as resulting from the interaction in which participating donor and acceptor ions are both Pr^{3+} ions in the same $^1D_2$ excited state. Through this interaction process donor ions de-excite into the $^1G_4$ state and release enough energy to up-convert the acceptor ion to the $^3P_2$ state, which then relaxes rapidly into the $^3P_0$ level from which emission occurs. In the KPP system this process occurs with the emission of 531 cm^{-1} phonons, and can be written as

$$[^1D_2(1),\ ^1D_2(1)] \rightarrow [^3P_2(5),\ ^1G_4(9)] + 531\ cm^{-1}. \tag{11}$$

A schematic representation of this cooperative energy transfer is presented in figure 9.

The up-converted $^3P_0$ fluorescence of Pr^{3+} ions after pulsed $^1D_2$ excitation has also been observed in other materials: $LaF_3:Pr^{3+}$ by Vial *et al* (1979), Lai *et al* (1982) and in $CaF_2:Pr^{3+}$ by Lezama *et al* (1985), but to our knowledge this is the first observation of up-conversion processes in concentrated and stoichiometric RE phosphates.

According to equation (11) only Pr^{3+} pairs can participate in the up-conversion transfer. This is confirmed by our excitation spectra of the $^3P_0$ emission measured as a function of dye laser frequency. A clear pair excitation spectrum of the $^1D_2(1)$ level has been observed for KYP : 3% Pr^{3+} (2 μs delay) when no evident changes in the excitation line profiles of the $^1D_2$ and $^3P_0$ emission in stoichiometric KPP were found. We thus conclude that the up-conversion process takes place by energy transfer between strongly coupled, neighbouring Pr^{3+} ions simultaneously excited by the laser pulse. It is also interesting to note that the trap Pr^{3+} ions participate in this up-conversion and that the ratio of the trap and intrinsic line intensity in excitation spectra of the $^1D_2$ and $^3P_0$ fluorescence are, for given Pr^{3+} concentrations, roughly the same.

The temporal behaviour of the blue fluorescence under $^1D_2(1)$ excitation is governed mainly by the transfer rate W_t and the radiative decay rates W_2 and W_3 of the $^1D_2$ and $^3P_0$ fluorescence, respectively (see Vial *et al* 1979). The non-radiative cascade from the $^3P_2$ to $^3P_0$ state is very fast; from our earlier data (Malinowski 1985) we could expect in this case an energy transfer rate as large as $10^8\ s^{-1}$. The rate equation for this cooperative energy transfer among Pr^{3+} ions is

$$dN_3/dt = -N_3W_3 + W_tN_2^2 \tag{12}$$

where N_3 is the population of the $^3P_0$ state. With the initial conditions $N_3(0) = 0$, using N_2 defined by equation (4) and assuming that $W_3 \gg W_2$ and W_{t2}, the fluorescence decay of the $^3P_0$ level should take the form

$$N_3 = \frac{W_t}{W_3}\left(\frac{N_{20}}{W_{t2} + W_b + 2W_2}\right)^2 (\{W_b \exp(-W_2t) + W_{t2} \times \exp[-(W_2 + W_{t2} + W_b)t]\}^2 + (W_b + W_{t2})^2 \exp(-W_3t)). \tag{13}$$

Utilising $W_3 = 1.54 \times 10^6\ s^{-1}$ obtained under direct excitation of the $^3P_0$ state at 4.4 K and the values of W_2 and W_b determined earlier, we fitted equation (13) to the observed fluorescence decay. However, in the discussed model no satisfactory agreement with experimental results could be obtained, the departures being especially large for times longer than about 50 μs when the slow component in the decay of the blue fluorescence appeared. The complicated form of the up-converted $^3P_0$ emission could be interpreted by taking into account the up-converted delayed signal from traps. Utilising N_2, in the form given by equation (5) we could solve equation (12) and obtain the relative $N_{3'}(t)$, which is shown in figure 8 together with the observed temporal variation in the blue emission.

$$N_{3'} = \frac{W_t}{W_3}\left(\frac{N_{20}W_{t2}}{W_{t2} + W_b + 2W_2}\right)^2 (\{\exp(-W_2 t) - \exp[-(W_2 + W_{t2} + W_b)t]\}^2 + \exp(-W_3 t)). \tag{14}$$

Good agreement was obtained for $KYP:Pr^{3+}$ samples with $x < 0.85$; the resulting W_t values as a function of Pr^{3+} concentration are shown in figure 10. From figure 10 it follows that at higher temperatures the quenching of luminescence and up-conversion transfer become explicit above $x = 0.2$. This value is close to the so-called critical concentration for lattice percolation (Kopelman 1976), i.e., $x = 0.31$ for a simple cubic lattice. At this concentration all clusters are connected and processes involving more than two ions predominate.

The trap model, however, could not explain the complicated shape of the up-converted $^3P_0$ fluorescence decay in KPP. In this stoichiometric crystal one could clearly observe the strongly delayed component with the rise-time of about 25 μs (see figure 8). Further studies of this phenomena are being conducted at our laboratory.

5. Conclusion

We have demonstrated that several processes contribute to the quenching of the $^1D_2$ fluorescence of Pr^{3+} ions in the $KPr_xY_{1-x}P_4O_{12}$ system. It was shown that in mixed $KYP:Pr^{3+}$ crystals at low temperature the fluorescence is strongly affected by energy transfer to radiative traps. In diluted crystals most of the fluorescence originates from non-regular trap ions. The presence of intense $^1D_2$ emission observed in stoichiometric KPP crystals is an indication of the weakness of concentration-dependent fluorescence quenching in Pr^{3+} tetraphosphates. Investigations of the shape of $^1D_2$ decay lead to the conclusion that a direct transfer to acceptors dominates the quenching mechanism at 4.4 K and that this interaction is short-range in nature. The decay characteristics may be understood in terms of the short-range superexchange interaction between nearest-neighbour ions and electric dipole–quadrupole coupling for more distant species. Anti-Stokes $^3P_0$ fluorescence observed under excitation of the $^1D_2(1)$ level is related to the cooperative two-ion process. The temporal evolution of this fluorescence is successfully predicted taking into account the up-converted trap emission.

Although much progress has been achieved in understanding the problem of $^1D_2$ fluorescence quenching in Pr^{3+} phosphates, further work is still required to obtain a general understanding of this process. Szymański (1983), for example, found that the oscillator strengths of the $^3P_0$ and $^1D_2$ transitions in Pr^{3+}-doped LaP_5O_{14} are strongly concentration dependent. This means that the quenching mechanism, first proposed by

Danielmeyer (1976) and then demonstrated by Auzel (1976) is inactive in the case of Nd^{3+} phosphates through crystal field overlap mixing effects (CFOM), yet could be active in the case of concentrated Pr^{3+} compounds.

Acknowledgments

The author gratefully acknowledges the hospitality and support offered by the Laboratorie de Physico-Chimie de Materiaux Luminescents, CNRS, Lyon. It is a pleasure to thank Dr A Monteil for sharing with the author his computer programs. This work has been partially supported by the CPBR 8.14 program.

References

Auzel F A 1976 *IEEE J. Quantum Electronics* **12** 258
Bartoli F J, Allen R E and Esterowitz L 1979 *Appl. Opt.* **18** 3365
Broer M M, Huber D L, Yen W M and Zwicker W K 1984 *Phys. Rev.* B **29** 2382
Danielmeyer H G 1976 *J. Lumin.* **12/13** 179
Dornauf H and Heber J 1979 *J. Lumin.* **20** 271
—— 1980 *J. Lumin.* **22** 1
Hong H Y-P 1975 *Mater. Res. Bull.* **10** 1105
Huber D L 1979 *Phys. Rev.* B **20** 2307
Huber G 1980 *Miniature Neodymium Lasers* (Current Topics in Materials Sciences vol XX) ed. E Kaldis (Amsterdam: North-Holland) p 1
Kopelman R 1976 *Radiationless Processes* ed. F K Fong (Berlin: Springer)
Lai Shui T, Shihua Huang and Yen W M 1982 *Phys. Rev.* B **26** 2349
Lawson C M, Powell R C and Zwicker W K 1982 *Phys. Rev.* B **26** 4836
Lempicki A and McCollum B C 1979 *J. Lumin.* **20** 291
Lezama A, Oria M and de Araujo Cid B 1986 *Phys. Rev.* B **33** 4493
Malinowski M 1985 *Proc. Int. Symp. Rare Earth Spectroscopy, Wroclaw*, ed. B Jeżowska-Trzebiatowska, J Legendziewicz and W Stręk (Singapore: World Scientific) p 348
—— 1986 *Phys. Rev.* B **34** 7578
—— 1989 *J. Phys. Chem. Solids* at press
Malinowski M, Jacquier B, Boulon G and Woliński W 1988 *J. Lumin.* **39** 301
Malinowski M and Stręk W 1987 *J. Phys. C: Solid State Phys.* **20** 2595
Malinowski M, Wolski R and Woliński W 1986 *J. Lumin.* **35** 1
Mazurak Z, Łukowiak E, Jeżowska-Trzebiatowska B, Schultze D and Waligóra Ch 1984 *J. Phys. Chem. Solids* **45** 487
Miyazawa S, Koizumi H, Kubodera K and Iwasaki H 1979 *J. Cryst. Growth* **47** 351
Szymański M 1983 *J. Lumin.* **28** 87
—— 1984 *J. Lumin.* **29** 433
Vial J C, Buisson R, Madeore F and Poirier M 1979 *J. Physique* **40** 913